Biochimica et Biophysica Acta 1834 (2013) 2554–2563

Contents lists available at ScienceDirect

Biochimica et Biophysica Acta

journal homepage: www.elsevier.com/locate/bbapap

Cooperative dynamics of a DNA polymerase replicating complex

Samuel L.C. Moors [a,*], Piet Herdewijn [b,1], Johan Robben [c,2], Arnout Ceulemans [a,3]

[a] Department of Chemistry, KU Leuven, Celestijnenlaan 200F, B-3001 Leuven, Belgium
[b] Rega Institute for Medicinal Research, KU Leuven, Minderbroedersstraat 10, B-3000 Leuven, Belgium
[c] Department of Chemistry, KU Leuven, Celestijnenlaan 200G, B-3001 Leuven, Belgium

ARTICLE INFO

Article history:
Received 25 April 2013
Received in revised form 22 August 2013
Accepted 6 September 2013
Available online 13 September 2013

Keywords:
Replica exchange with flexible tempering
DNA polymerase
Protein–DNA interaction
Thermococcus gorgonarius

ABSTRACT

Engineered DNA polymerases continue to be the workhorses of many applications in biotechnology, medicine and nanotechnology. However, the dynamic interplay between the enzyme and the DNA remains unclear. In this study, we performed an extensive replica exchange with flexible tempering (REFT) molecular dynamics simulation of the ternary replicating complex of the archaeal family B DNA polymerase from the thermophile *Thermococcus gorgonarius*, right before the chemical step. The convoluted dynamics of the enzyme are reducible to rigid-body motions of six subdomains. Upon binding to the enzyme, the DNA double helix conformation changes from a twisted state to a partially untwisted state. The twisted state displays strong bending motion, whereby the DNA oscillates between a straight and a bent conformation. The dynamics of double-stranded DNA are strongly correlated with rotations of the thumb toward the palm, which suggests an assisting role of the enzyme during DNA translocation. In the complex, the primer–template duplex displays increased preference for the B-DNA conformation at the n − 2 and n − 3 dinucleotide steps. Interactions at the primer 3′ end indicate that Thr541 and Asp540 are the acceptors of the first proton transfer in the chemical step, whereas in the translocation step both residues hold the primer 3′ terminus in the vicinity of the priming site, which is crucial for high processivity.

1. Introduction

Reproduction of a living cell relies on the replication of its genetic material. DNA polymerase (pol) enzymes catalyze the faithful replication of DNA in vivo. Deoxyribonucleotides (dNTP) are attached to the 3′ hydroxyl of a DNA primer strand, which is paired to a complementary template strand, to form a double-stranded DNA (dsDNA) helix.

All B-family pols share a similar polymerase active site pocket, the so-called "right hand" fold, which consists of a palm, fingers and thumb domain. Many also possess a 3′–5′ exonuclease proofreading domain, two notable exceptions being the eukaryotic pol α and pol ζ.

Archaeal family B pols are attractive tools in molecular biology methods such as PCR and cloning because of their extreme thermostability and high replication fidelity, which is attributed to their intrinsic proofreading activity [1]. Archaeal family B pols have been successfully engineered to make them receptive to various synthetic nucleic acid substrates, containing modifications in the bases as well as in the sugar-phosphate backbone [2]. Recent examples are the synthesis of DNA from nucleoside triphosphate analogs containing phosphoramidates as pyrophosphate mimetics [3], and the synthesis and replication of DNA-based polymers using fluorescent dye-labeled dC bases [4].

Rational design of polymerases for improved or altered activities requires detailed knowledge of their functional dynamics and the specific protein–substrate interactions. To this end, molecular dynamics (MD) simulation can complement experimental data by providing insight into the dynamics at atomic resolution. To date however, conventional MD simulation is unable to fully capture the complex, long-time, large-scale conformational changes that take place during catalysis.

In cases where X-ray crystal structures at different states of the catalytic cycle are available, transition pathways can be generated with biased MD methods that drive the system from the initial state toward the final state along predefined coordinates. Radhakrishnan and Schlick [5] used targeted MD to generate an initial path along the transition between the open and closed states of the pol β ternary complex, after binding of the incoming dNTP. Analysis of the generated pathway led to the identification of four metastable transition state regions, which were used as start and end regions for multiple transition path sampling runs. Golosov et al. [6] focused on the translocation step after the chemical incorporation step in pol I. Here, restricted perturbation targeted MD was used to drive the translocation of the primer–template DNA. Da et al. [7] used steered MD to generate initial pathways for pyrophosphate (PPi) release in RNA polymerase II. Next, selected conformations along these pathways were used as starting points for 122 6-ns unbiased MD trajectories, which in turn were used to construct a Markov

* Corresponding author at: Center for Molecular Modeling, Ghent University, Technologiepark 903, B-9052 Zwijnaarde, Belgium. Tel.: +32 9 264 66 37.
E-mail addresses: samuel.moors@ugent.be (S.L.C. Moors), piet.herdewijn@rega.kuleuven.be (P. Herdewijn), johan.robben@chem.kuleuven.be (J. Robben), arnout.ceulemans@chem.kuleuven.be (A. Ceulemans).
[1] Tel.: +32 9 264 66 37.
[2] Tel.: +32 16 3 27316.
[3] Tel.: +32 16 3 27363.

1570-9639/$ – see front matter © 2013 Elsevier B.V. All rights reserved.
http://dx.doi.org/10.1016/j.bbapap.2013.09.003

state model to simulate the PPi release process along the secondary channel.

To date however, a crystal structure of the replicating complex of an archaeal family B pol has not yet been reported. Even less is known about the structural dynamics of the replicating complex, which are essential for its function. Furthermore, conformational states of flexible proteins in solution cannot be fully described by a single experimental structure in the crystalline state. On the other hand, extensive Boltzmann-weighted conformational state ensembles contain detailed information of the important interactions as well as the global motions, which provide direct evidence of the transition pathways in an unbiased way.

In this report, to investigate the dynamics upon DNA and nucleotide substrate binding, and to gain insight into the polymerase reaction mechanism, we applied the replica exchange (RE) with flexible tempering (REFT) method to *Thermococcus gorgonarius* (Tgo) pol complexed with primer–template DNA and dTTP in explicit solvent, right before the primer extension. The starting structure for this simulation was obtained by modeling the primer–template DNA and dTTP into the polymerase active site of the apo-protein. The dynamics were analyzed by principal component analysis (PCA) and compared with the dynamics from a set of X-ray structures of Tgo pol close analogs, with a set of bacteriophage RB69 (gp43) pol X-ray structures, and with an MD simulation of the unbound dsDNA in solution.

2. Methods

2.1. Construction of the ternary complex

The initial coordinates were taken from the X-ray crystal structure of Tgo pol (PDB ID: 1tgo) [8]. The flexible C-terminal tail, comprising residues 751–773, was removed. Primer–template DNA, dTTP and three polymerase active-site Ca^{2+} ions from the RB69 pol replicating complex X-ray crystal structure [9] (PDB ID: 1ig9) were added by structural alignment of the RB69 pol and Tgo pol palm domains. The Ca^{2+} ions were replaced by Mg^{2+}. Steric clashes between the DNA and the protein were alleviated by alternative side chain rotamers. Side chains of residues directly interacting with the Mg^{2+} ions (Asp404, Asp542, Glu580) were rotated to align with the corresponding 1ig9 side chains. The dideoxy-C at the 3′ terminus was converted into dC by adding the 3′-hydroxyl group to this nucleotide. To reduce system size and to avoid possible denaturation at high temperature, the primer and template strands were shortened and linked together using the X-ray crystal structure of Tgo pol (PDB ID: 2vwj) [10] as a template. The final self-hybridized DNA 23-mer sequence, 5′-d(ACAGGTAAGCC**TTTT**GGCTTACC)-3′, consists of 8 base pairs, which are connected by a 4-nucleotide hairpin loop (bold), and has a 3-nucleotide 5′ template extension (underlined).

2.2. MD simulation setup

The ternary complex was neutralized with Na^+ ions, and solvated in a dodecahedral box with 35,559 water molecules. For the simulation of the unbound dsDNA, the 5′-overhang was removed. Na^+ counter ions and 6492 water molecules were added in a periodic dodecahedral box. Molecular dynamics (MD) simulations were performed using a modified version of the open-source GROMACS 4.0 software package [11], which allows for Hamiltonian and temperature exchanges between replicas. The AMBER ff99SBildn [12] and ff99bsc0 [13] force fields were used for the protein and the DNA, respectively. Force field parameters for dTTP were adapted from dT, using the phosphate parameters from ATP [14]. Long-range electrostatics were computed with the particle mesh Ewald method. The non-bonded cutoff was set to 1.0 nm. A Fourier spacing of 0.16 nm was used. All covalent bonds were constrained using P-LINCS. The integration time step was 2 fs. The neighbor list was updated every 10 steps. The temperature was controlled by the velocity rescaling thermostat. After a steepest descent minimization of 50,000 steps, the system was heated to 300 K with position restraints and equilibrated for 2 ns.

2.3. Replica exchange with flexible tempering

The REFT method [15] is a combination of Hamiltonian and temperature replica exchange molecular dynamics, an extension of the RE with solute tempering (REST) method [16]. In REST, the solvent molecules in the high-temperature replicas are effectively kept in a low-temperature state. Although REST is an improvement over conventional RE in that much less replicas are required to obtain similar exchange probabilities, it suffers from a decoupling between the high (unfolded) and low (folded) temperature replicas. This decoupling is due to the slow refolding process, which is necessary to travel from the high temperature to the low temperature replicas [17]. In REFT, the set of atoms in this cold state is extended to include the rigid domains of the protein. REFT has the advantage that much less replicas are required for a given temperature range, because only the flexible parts of the solute are effectively heated up. Moreover, as the solute maintains a native-like conformation even at high temperatures, the rate of replicas crossing the entire temperature range is greatly enhanced, yielding substantially improved sampling efficiency [15]. A detailed description of REFT and analysis of its performance can be found in our previous work [15]. Generally, all atoms of the system are categorized as either "hot" (h) or "cold" (c). The total energy E_0 is defined by the interactions between the hot and cold atoms:

$$E_0 = E_{h-h} + E_{c-c} + E_{h-c}. \quad (1)$$

Each replica i uses a potential energy function that is dependent on the system temperature:

$$E_i = E_{h-h} + (\beta_0/\beta_i)E_{c-c} + \sqrt{\beta_0/\beta_i}E_{h-c} \quad (2)$$

where $\beta = 1/k_BT$. In REFT, the flexible atoms of the solute are treated as "hot", while the solvent and rigid parts of the system are "cold".

In the ternary complex, rigid and flexible protein atoms were determined using FIRST [18] with a constraint cutoff energy of -1.2 kcal mol^{-1}. This cutoff energy yielded 13 rigid domains, comprising 30% of all protein atoms. The DNA and dTTP atoms were treated as "cold". In our REFT MD simulation, 25 replicas were used. Replica temperatures ranged between 350 K and 500 K. The lowest replica temperature (350 K) corresponds to the midpoint of the Tgo growth range [8]. Pairwise exchanges were attempted every 1 ps, and acceptance rates ranged between 0.14 and 0.16. Starting coordinates for REFT were sampled from a 2 ns MD simulation at 500 K with corresponding potential function. The total REFT simulation time was 420 ns per replica. As shown in Figs. S1 and S2 (supplementary information), frequent temperature crossing is observed between the high and low temperature replicas. The last 360 ns of the lowest temperature replica were used for averages and PCA analysis.

2.4. Homology modeling

Homology modeling was performed with Nest [19], a program that is capable of generating homology models from multiple reference structures. Tgo pol models of Tgo pol analogs were generated from two reference structures. The Tgo pol analog was used as the primary reference. Tgo pol was used as the secondary reference in regions where the sequences could not be aligned, and in regions where Tgo pol analog has missing backbone coordinates.

2.5. Analysis

The following cutoff criteria for H-bonds were used: donor–acceptor distance ≤ 0.35 nm, acceptor–hydrogen–donor angle $\leq 30°$. For salt

bridges, only the distance cutoff was used. For the analysis of DNA parameters, 8 base pairs were used starting at the 3′ primer end. DNA axis bending angles were computed with the program Curves+ [20]. The structural parameters z_P, slide and χ were calculated with 3DNA (v2.0) [21]. PCA analysis was performed on and after fitting the protein Cα atoms to those of the modeled complex. Protein domains and hinge axes were determined from the PCA eigenvector motions with the program DynDom [22], setting the window length and minimum domain size to 3 and 28, respectively. The numbering of α-helices and β-strands in Tgo pol was adopted from Hopfner et al. [8]. Reported statistical errors were calculated using the Gromacs g_analyze block averaging tool.

3. Results

The initial ternary replicating complex was constructed from 1tgo, an apo Tgo pol crystal structure in a closed conformation [8]. In the ternary replicating complex, the complex is expected to be also in a closed conformation. We thus anticipate that an extended REFT simulation will reveal if the closed 1tgo conformation is representative for the polymerase mode, or if the enzyme and the primer–template DNA further adapt to accommodate each other and to optimize the intra- and intermolecular interactions.

3.1. Overall structure of the replicating complex

The overall structure of Tgo pol is folded into five distinct domains [8] (Fig. 1): the N-terminal domain (N-term, residues 1–130), the 3′–5′ exonuclease domain (exo, 131–326), the palm (369–449 and 500–585), the fingers (450–499), the thumb (586–773), and a helical interdomain linker which connects the exo and palm domains (interdomain, 327–368). The thumb is subdivided into the thumb base (thumb1, 586–655 and 728–773) and the thumb tip (thumb2, 656–727).

In the ternary complex at 350 K, Tgo pol maintains its overall fold throughout the simulation. The total protein conformation stays within 0.45 nm Cα root mean square deviation (rmsd) from the minimized X-ray structure. The major domains and most X-ray secondary structure elements are preserved. The eight dsDNA primer–template Watson–Crick base pairs remain largely intact.

Interactions of the Mg^{2+} ions with the protein and incoming nucleotide are generally analogous to the RB69 pol crystal structure. The average coordination number of the three Mg^{2+} ions is around five. MGA is coordinated with two water molecules, the dTTP α and γ phosphates, and the Asp542 sidechain. MGB is coordinated with the β and γ phosphates, the Asp404 and Asp542 sidechains, and partially with the Phe405 carbonyl (67%) and one water molecule (43%). MGB is coordinated with three water molecules and with the Asp404 and Glu580 side chains.

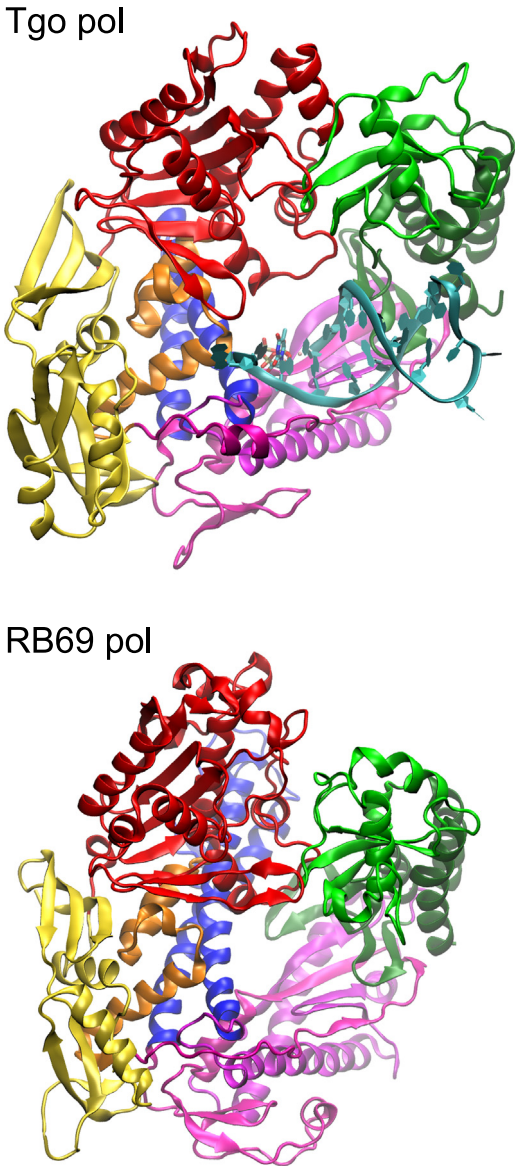

Fig. 1. Upper: crystal structure of Tgo pol (1tgo), with primer–template DNA (cyan) and incoming dTTP nucleotide (sticks) modeled into the polymerase active site. Lower: crystal structure of the RB69 pol replicating conformation (1ig9), without the DNA/dTTP substrates. Coloring of the protein structural domains is similar to Ref. [8]: N-term (yellow), exo (red), interdomain (orange), palm (magenta), fingers (blue), thumb1 (dark green), thumb2 (light green).

3.2. Flexibility of the replicating complex

Analysis of the Cα root mean square fluctuation (rmsf) shows that the most flexible parts of the protein are located in the exo and thumb2 domains (Fig. 2A). Notable flexible regions in the exo domain are seen at the interface with thumb2: helix H + loop αH–αI (residues 291–304), and loop β10–β11 (148–152), and in the β-hairpin motif (245–246), which acts as a wedge between the primer and the template in the editing complex [23]. Four flexible loops make close contact with the dsDNA, three of which are located in the thumb: loop αM–β16 (379–381), loop β24–β25 (610–613), loop β26–αU (672–677), and loop β27–β28 (707–712). The rmsf of the dsDNA backbone C3′ atoms with respect to the protein is lowest at the primer n − 2 and n − 3 sites, and increases with the distance from the polymerase active site (Fig. 2B).

The structural parameter z_P has been reported as the best discriminator to distinguish B-DNA (<0.5), A-DNA (>1.5), and conformational intermediates along the B to A transition pathway (AB-DNA) [24]. The z_P parameter is defined as the mean of z-coordinates of the four backbone phosphorus atoms with respect to a dimer reference frame. In Fig. 3, the average z_P at each dinucleotide step is compared between the enzyme-bound and a 200 ns MD simulation of free unbound dsDNA. In the free dsDNA, the highest degree of B-DNA is found at the midpoint of the chain (n − 4 to n − 5). Deviations from symmetry are due to the asymmetric DNA sequence and the presence of the hairpin loop. The tendency of the complex to adopt a B-DNA conformation is highest at the n − 2 to n − 3 step, and significantly higher than that of the free dsDNA. The same trend (albeit less pronounced) is observed with the slide and χ parameters (Fig. S3). On the other hand, at longer distances from the catalytic center, the propensity for a B-DNA conformation is much lower. This tendency for A-DNA coincides with a widening of minor groove (Fig. S4). The increased groove width is stabilized by strong interaction with loop β24–β25 (610–613); the hydrophobic

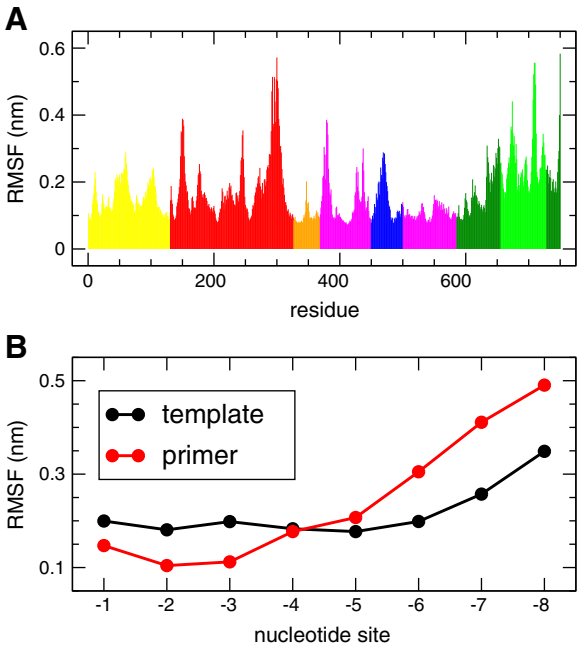

Fig. 2. (A) Protein Cα rmsf as a function of residue number, with coloring of structural domains as in Fig. 1. (B) Primer and template C3′ rmsf as a function of nucleotide site.

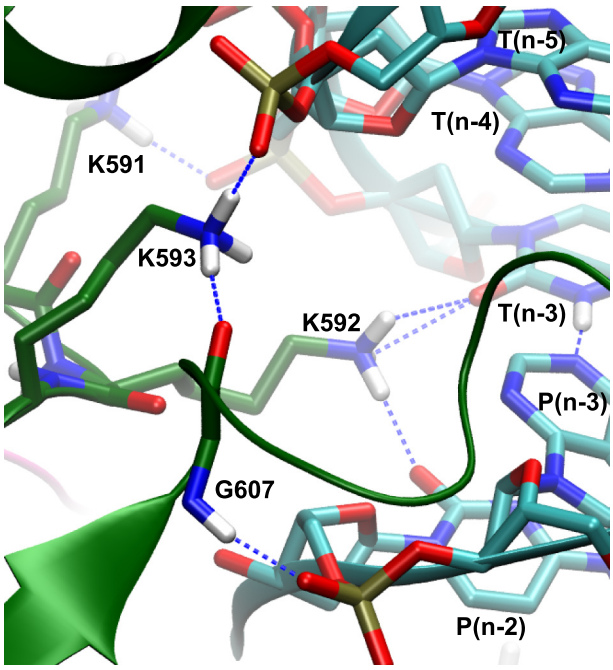

Fig. 4. Snapshot showing the B-DNA stabilizing H-bond network P(n − 2) phosphate–Gly607–Lys593–T(n − 6) phosphate. Also shown are the H-bond interactions between Lys592 and the P(n − 2) and T(n − 3) bases.

Val611 sidechain is located inside the minor groove, while Arg612 and Arg613 form salt bridges with the template and primer phosphates, respectively. At steps n − 6 to n − 8, the average z_P value corresponds to an intermediate AB-DNA conformation.

The high preference for the B-DNA conformation at the n − 2 to n − 3 and n − 3 to n − 4 steps is due to strong electrostatic interactions with the enzyme. In the RB69 pol replicating complex, the conserved KKRY motif (K591KKY in Tgo pol) has been suggested to stabilize the B-DNA conformation [9]. In our Tgo pol solution ensemble, in addition to the KKKY motif, several residues located in the exo, palm and thumb provide additional stabilization of the DNA backbone in the n − 2 to n − 4 region (Tables S1 and S2). Of special notice is the H-bond network involving the highly conserved Gly607 (Fig. 4). Gly607 is H-bonded via its amide N–H with the primer n − 2 phosphate and via its carbonyl oxygen with the Lys593 side-chain, which in turn forms a salt bridge with the template n − 6 phosphate. This H-bond network stabilizes the narrow minor groove, which is characteristic for B-DNA.

The single-stranded DNA (ssDNA), at the 5′ extension of the template strand, is very mobile; its conformational ensemble is divided between an extended state, where it is located in the template strand binding region, and a curled state, where it is folded onto the dsDNA. This high ssDNA mobility is explained by the short length (3 nucleotides) of the single-stranded template extension, and the missing phosphate at the template 5′ end.

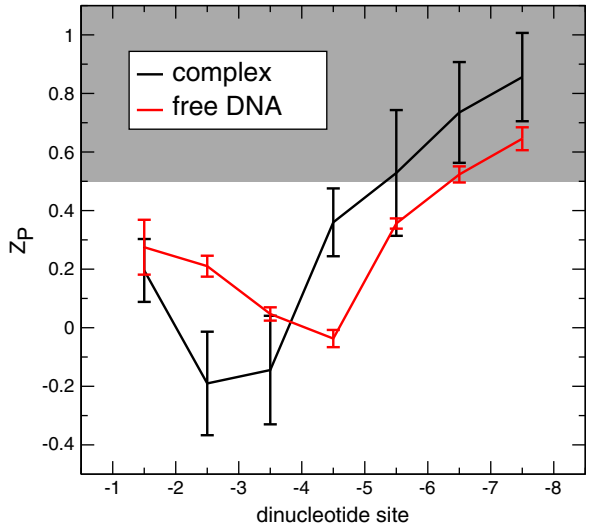

Fig. 3. dsDNA zP values taken as an average and standard error over the simulation as a function of the dinucleotide step in the complex and in the unbound state. The region with intermediate AB-DNA conformation is shown in gray.

3.3. Global dynamics in solution

We analyzed the global protein dynamics by PCA, using the Cα atoms of the residues in the α-helices and β-sheets, excluding two small helices with high mobility (residues 292–300 and 374–377). Prior to the PCA, all snapshots were fitted onto the X-ray structure using the same Cα atoms. The purpose of this coordinate subset was to obtain a clear view of the rigid domain motions, free from the dynamics of the flexible loops, tails and side chains. The first five PCA eigenvectors account for a summed variance of 6.0 nm^2 out of a total variance of 9.3 nm^2 (Fig. S5A). Each eigenvector mode is characterized by rotating domains and hinge axes with the Dyndom program (Fig. 5). Movies S1 to S5 of the motions along the eigenvectors are provided in supplementary material. The projections of the MD trajectory onto the protein eigenvectors are shown in Fig. S6.

The first three eigenvector modes involve a rotation of the thumb toward the palm, effectively wrapping around the dsDNA, but with different positions and orientations of the rotation axes (Fig. 5). In mode 1, the thumb rotates sideways relative to the palm about the axis with a blue arrow head. Simultaneously, a second axis (yellow arrow head) divides the N-term into 2 sub-domains: N-term1 (residues 1–31 and 119–130) and N-term2 (37–118). N-term2 rotates relative to the exo, N-term1 and fingers domains, which in turn rotate relative to the palm about the third axis (green arrow head). In the second mode, the

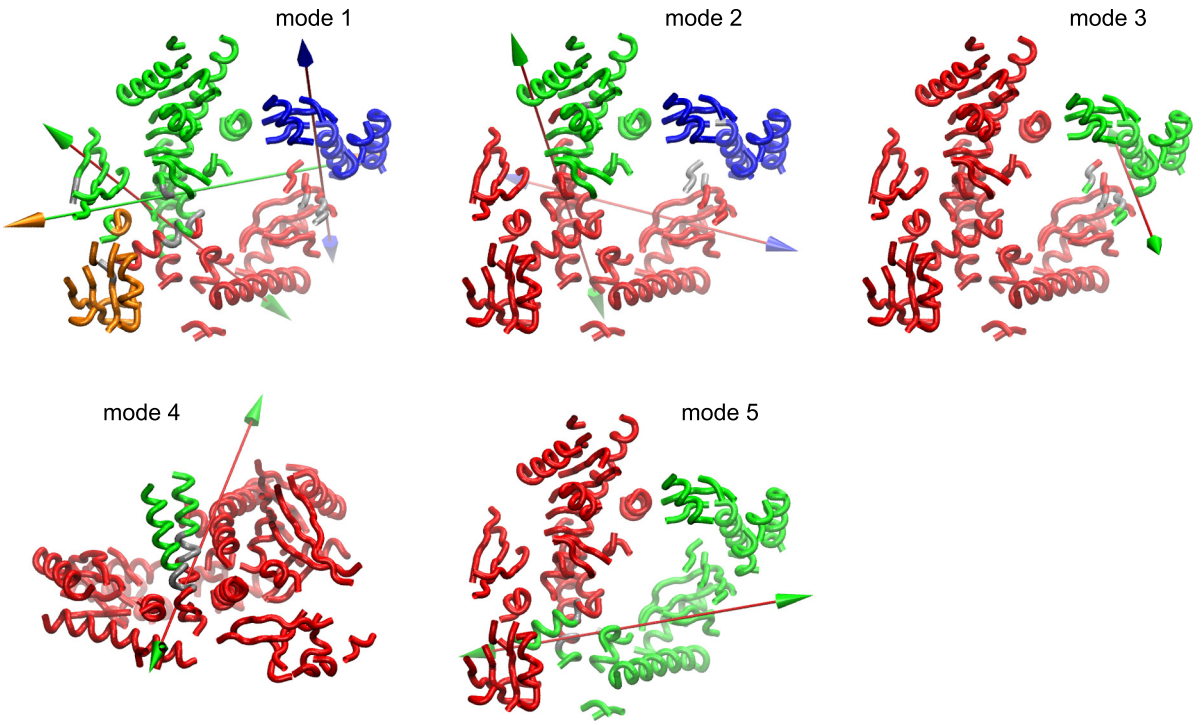

Fig. 5. DynDom analysis of the first five PCA modes from the REFT MD simulation of Tgo pol. The protein α-helices and β-sheets plus the DNA backbone are shown in the same orientation as Fig. 1, except for mode 4. Independently rotating domains are colored red, green, blue and orange. Hinge residues are colored gray. The hinge axes, which define the rotation between two independent domains, are indicated by arrows; the colors of the shaft and head correspond with the rotating domains.

thumb rotates toward helix Q of the palm, while at the same time the exo rotates away from the thumb. Mode 3 represents a thumb rotation away from the exo domain and toward the dTTP nucleotide.

In mode 4, the fingers domain rotates toward/away from the palm with a maximum rotation angle of 40°. Interestingly, during this rotation, helix P remains bound to helix I of the helical interdomain, with helix O making the largest spatial displacement. This is evidenced by the position of the hinge axis, which runs along the interface between helices P and I. Important fingers–interdomain interactions are the salt bridges Arg482–Glu332 and Lys477–Glu325, and a large hydrophobic cluster (interdomain residues 328, 329, 333, 336, 337, 354, 356, and fingers residues 481, 486, 488, 489). In addition, no net change of mode 4 was observed upon formation of the complex. Rather, the fingers hinge rotation angle fluctuates around the X-ray starting conformation (Fig. S6), which highlights the dynamic nature of this mode. Mode 5 corresponds to an opening-closing motion of the thumb and the palm relative to the N-term, exo and fingers domains. This mode resembles the opening-closing mode between the apo and binary editing complexes seen in the archaea crystal structures (see below).

The fingers domain plays an important role in recognition of the incoming nucleotide. Kinetic studies of DNA polymerization by *Sulfolobus solfataricus* P2 pol B1 at 37 °C have revealed a rate-limiting conformational change which precedes the chemical step [25]. The nature of this conformational change is still unknown. Based on crystal structures, Franklin et al. [9] have proposed the closing of the fingers toward the palm, which is required for optimal interaction with the nucleotide, as the rate-determining step in RB69 pol. On the other hand, Brown and Suo [25] have argued that the fingers motion may be too fast to be rate-limiting, which is the case for at least two family A DNA polymerases. Both seemingly opposing views may be reconciled if we consider that the fingers domain rotates at two different timescales. A fast, oscillating rotation of helix O is described by mode 4. Helix P, which accommodates the key dNTP-interacting residues, remains relatively inactive in this mode. On the other hand, mode 1 (and to a lesser extent, mode 5) establishes slow and likely rate-determining relaxation of three domains, fingers, exo and N-term, which collectively rotate toward the catalytic palm domain. This slow motion includes both helices O and P. Although PCA analysis does not directly provide information on the kinetics, an indication for the timescale difference can be incurred from the probability distributions. Mode 1 shows two clearly separated peaks in the distribution, (Fig. S6). A bimodal distribution indicates the presence of a barrier of activation, and thus slow kinetics. Mode 4, on the other hand, displays a more unimodal distribution (Fig. S6).

Likewise, we performed a PCA on the global dsDNA dynamics using the deoxyribose C3′ atoms of the eight base pairs. Two eigenvectors dominate the motions of the dsDNA. The first eigenvector describes a twisting motion during the first half of the simulation. Here, the dsDNA transforms from a twisted state to a partially untwisted state (Figs. 6A and S7). This transformation coincides with the rotation of thumb2 toward the palm domain, making strong interactions with the minor groove (Figs. S8A and S9A, B). This mode correlates well with protein MD mode 2 (Pearson correlation coefficient $R = -0.65$). The motion along the twisting vector is also highly correlated with the minor groove widths of dinucleotide steps $n - 4$ to $n - 7$ (R ranges between -0.82 and -0.91). In the untwisted state (second half of the simulation), eigenvector 2 traces strong bending motion of the helical axis (Fig. 6B). Two distinct conformational states are present along this vector. The dominant state has a straight helical axis. In the less populated state, the dinucleotide sites $n - 6$ to $n - 8$ are bent away from the thumb domain, toward the $n - 1$ to $n - 5$ sites. This bending mode corresponds with a rotation of thumb1 toward the palm (Fig. S8B), and correlates with protein MD modes 1 ($R = 0.68$) and 3 ($R = -0.69$). The absence of this bending motion in the twisted state indicates that partial untwisting facilitates bending of the DNA double strand.

Comparison with the free dsDNA dynamics clearly shows that the untwisted states are stabilized by the presence of the polymerase enzyme (Fig. S10). Although in the free dsDNA the untwisted states are sporadically sampled, the dominant conformation corresponds with the twisted state.

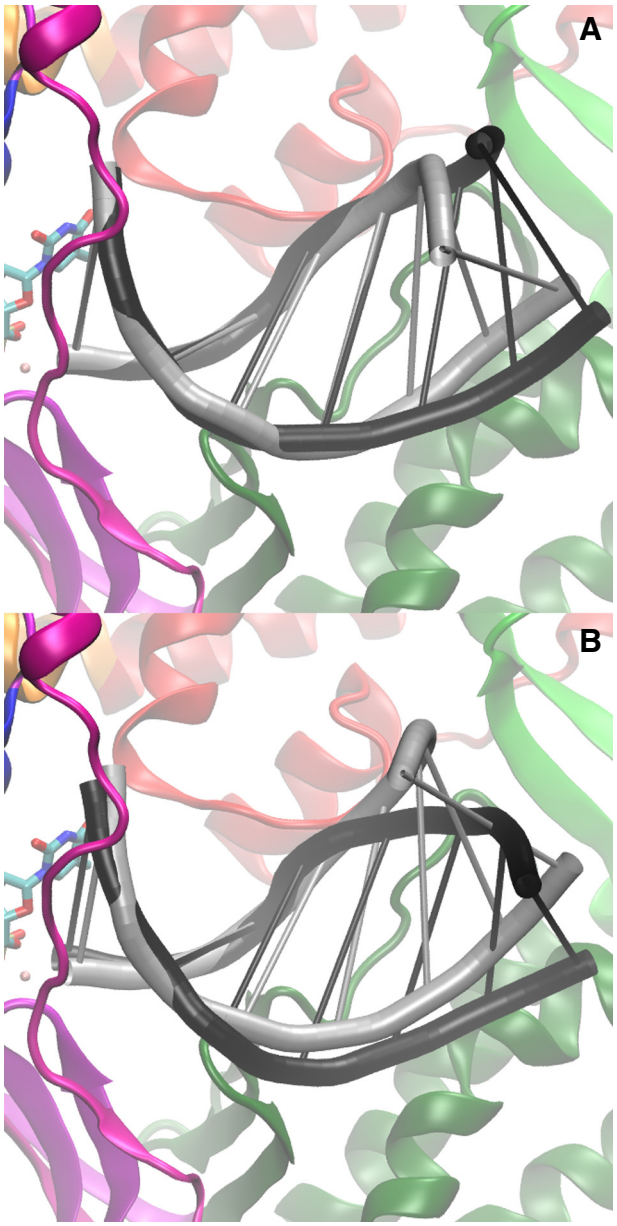

Fig. 6. Extremes along the (A) first and (B) second dsDNA eigenvectors overlayed onto the Tgo pol starting structure. The dsDNA C3′ backbone atoms are shown as black and gray tubes.

3.4. Global dynamics from archaea pol crystal structures

Comparison of the X-ray structures of Tgo pol and close archaeal pol analogs provides experimental evidence for the global dynamics of this group of proteins. A set of 11 X-ray structures were selected, which share ≥80% sequence identity with Tgo pol: 2 binary complexes in editing mode (PDB IDs: 2xhb and 2vwj) and 9 apo enzyme structures (PDB IDs: 1tgo, 2vwk, 1qht, 2jgu, 3a2f, 1wn7, 1wns, 1d5a, 1qqc and 1s5j). Performing a PCA of these analogs requires selecting an equal number of equivalent Cα atoms in all structures. To accomplish this, the analogs were mutated to Tgo pol by homology modeling. The PCA of the X-ray structures was done independently from the MD snapshots, and gives the best eigenvectors for the whole set.

In contrast to the PCA obtained from the MD data, just a few eigenvectors are required to describe the essential dynamics of the ensemble of X-ray structures (Fig. S5B). The two first eigenvectors combined account for a variance of 24.3 nm^2 out of a total variance of 26.9 nm^2. The reduced number of essential eigenvectors can be explained the limited number of low-temperature minimum energy conformations, and by the lack of replicating complexes in the set. Overlaps of the X-ray eigenvectors with those from MD provide an estimate of how well the X-ray modes are represented in MD and vice versa. As shown in Table 1, X-ray eigenvectors 1 and 2 overlap well with the subspace of the first five MD eigenvectors, although there is no clear one-to-one correspondence. X-ray eigenvector 1 has the highest overlap with MD eigenvectors 1 and 5; X-ray eigenvector 2 overlaps best with MD eigenvector 3.

The first X-ray PCA mode, with a variance of 21.5 nm^2 out of a summed total of 26.9 nm^2, reveals a rigid-body opening-closing motion of the thumb and a large part of the palm relative to the N-term, exo and fingers domains (Fig. 7A). The domain assignment in this mode is similar to MD mode 5, but the hinge axis is rotated by 41°. The hinge axis runs through the middle of palm helix Q and the root of fingers helix O. Extremely closed conformations are seen in the binary editing complexes. In the editing complexes, the overall shape of the protein matches a giant helix, with the exo and thumb domains interacting sideways with each other. Most apo structures adopt a very open conformation with a large frontal exo–thumb distance. The second mode (variance = 2.7 nm^2) involves a rotation of the thumb relative to the rest of the protein (Fig. 7A). Here the thumb rotates sideways toward/away from the exo, with the hinge axis perpendicular to the hinge axis of mode 1. This mode resembles MD mode 3, but the hinge axis is rotated by 29°. Two Tgo pol structures (1tgo and 2vwk) have a remarkably small sideways thumb–exo distance. In 1tgo and 2vwk, the thumb tip and exo domains make close frontal interactions, giving rise to a donut-like overall shape. In this thumb–exo arrangement, the thumb blocks access to the 3′–5′ exonuclease site. Both 1tgo and 2vwk have been crystallized in a solution with a high salt concentration (2 M ammonium sulfate), which may be the cause of their unusual closed conformation [8].

The projection of the MD snapshots onto the first two X-ray eigenvectors is represented by the red dots in Fig. 7A. In this conformational subspace, the protein samples a region that is located mostly above the 1tgo starting conformation, and includes 1d5a and the DNA sliding clamp complex (3a2f). The extremely closed and opened structures are not sampled, which suggests that the Tgo pol dynamics along the X-ray eigenvectors are strongly restrained by the presence of the DNA and dTTP substrates.

3.5. Global dynamics from RB69 pol crystal structures

The set of available archaeal pol X-ray structures lacks structures complexed with primer–template DNA in the polymerase mode, and does not fully capture the dynamics of the replicating complex. By contrast, many replicating complexes are available for RB69 pol. The topology of RB69 pol is very similar to Tgo pol (Fig. 1), despite a low sequence identity (17%). To compare the dynamics of the thermophilic Tgo pol with the mesophilic RB69 pol, a set of 27 RB69 pol X-ray structures was analyzed, containing 16 ternary replicating complexes, 6 binary complexes with the DNA bound in the polymerase active site, 4 apo enzymes and one binary editing complex. The PCA of this set was based on the Cα atoms of residues 1–888. The first and dominant mode (variance = 67.7 nm^2 out of 75.7 nm^2 in total) separates the replicating complexes from all other structures. This mode can be described

Table 1
Normalized PCA eigenvector overlaps of the REFT MD simulation and the X-ray crystal structures.

		MD				
		Vector 1	Vector 2	Vector 3	Vector 4	Vector 5
X-ray	Vector 1	0.27	0.14	0.00	0.02	0.33
	Vector 2	0.05	0.07	0.38	0.03	0.11

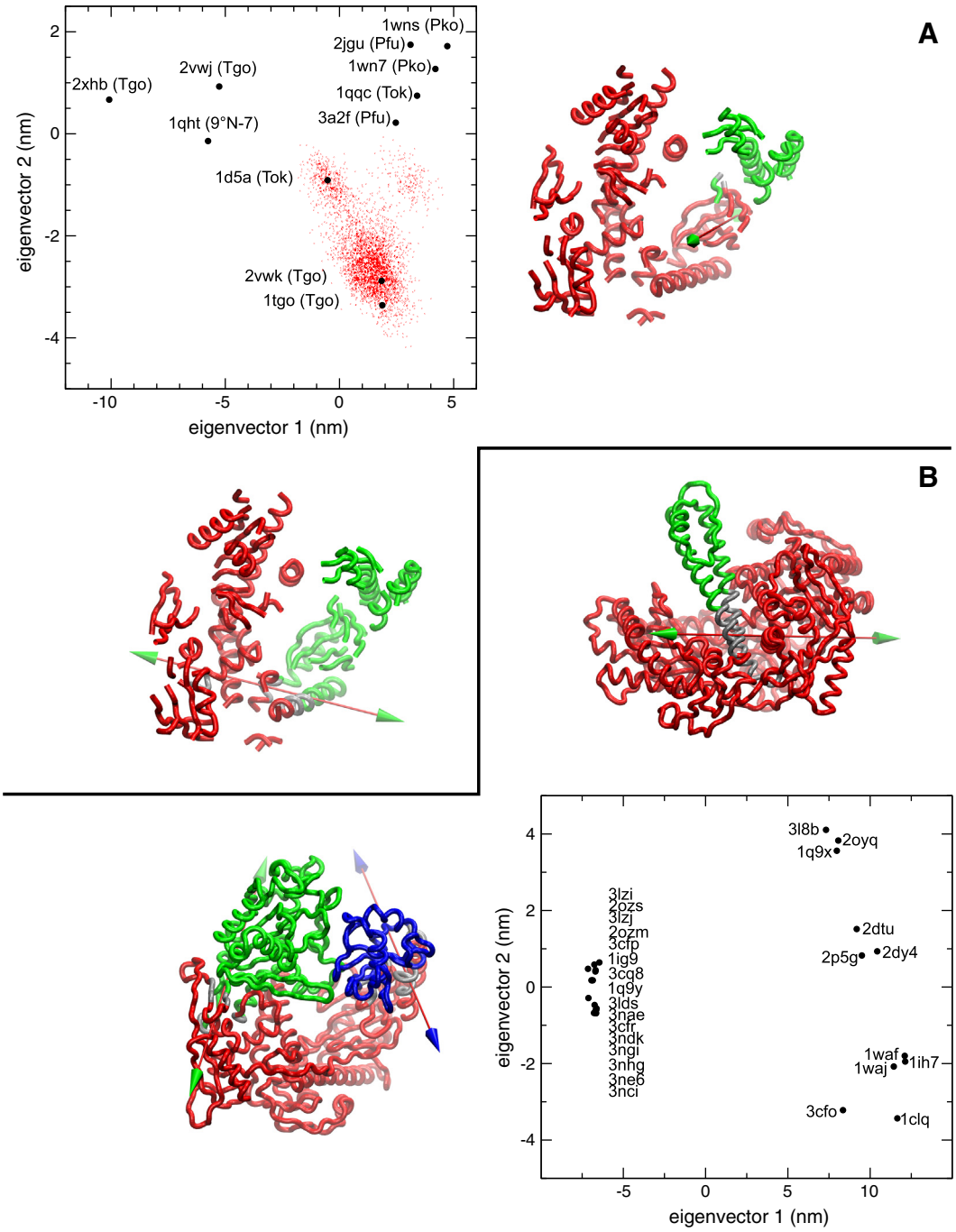

Fig. 7. Projection of the archaea pol (A) and RB69 pol (B) crystal structures on the first two PCA eigenvectors (black closed circles). The projection of the MD simulation onto the archaea pol eigenvectors is shown by red dots. Schematic representations of the modes are shown at the sides of their respective eigenvectors, in the same orientation as Fig. 1, except for RB69 pol mode 1, which is in the same orientation as the MD simulation mode 4.

by a rigid domain rotation of the fingers (Fig. 7B). In the replicating complexes, the fingers domain is rotated toward the palm to make strong interactions with the incoming nucleotide. The maximum rotation angle is 42°, similar to mode 4 of the Tgo pol MD PCA. However, in contrast to Tgo pol, the hinge axis is oriented perpendicular to the long axis of the fingers, which shows that the fingers rotation is not restrained by the nearby N-term or exo domains. In addition, in RB69 pol the fingers domain is much longer. Both factors contribute to a much larger displacement of the fingers relative to the Tgo pol MD.

The second mode (variance = 3.2 nm^2) is a concerted rotation of exo and thumb2, both moving in opposite directions relative to palm, N-term and fingers (Fig. 7B). This mode separates the binary polymerase-type complexes from the apo enzymes and the editing complex. In the former group of structures, thumb2 is rotated toward the palm and wrapped around the dsDNA, whereas in the latter group, the exo is rotated toward the palm. Thus, upon binding of the primer–template DNA and the incoming nucleotide, both the fingers (mode 1) and thumb2 (mode 2) rotate toward the palm to make close contact with the dsDNA and the nucleotide, respectively. While this result is similar to the solution dynamics of Tgo pol, here the motions of the fingers and thumb are much more localized and independent from the rest of the protein.

3.6. Protein–DNA interactions

Strong electrostatic interactions keep the dsDNA tightly bound to the palm and thumb domains. The average number of salt bridges between the dsDNA phosphate groups and cationic side chains increases to about 18 (Fig. S9C). A list of the most important DNA phosphate - protein salt bridge interactions is given in Table S3 (supplementary material). Remarkably, most cationic side chains make salt bridge interactions with two or more adjacent DNA phosphate groups, and many of these interactions are co-occurring. This finding may have important implications for DNA replication. The rate of DNA replication depends on the processivity as well as the pol-DNA binding affinity. The data in Table S1 suggest that the cationic side chains readily exchange salt bridge interactions with neighboring phosphate groups, thus facilitating fast DNA translocation while at the same time keeping the DNA tightly bound to the protein.

The highly conserved Lys592 side chain, located inside the minor groove, forms a remarkable H-bond with two DNA bases. A strong H-bond is formed with atom O2 of the primer base dC at the n − 2 position (71%). An additional H-bond or salt bridge is present between Lys592 and either atom O2 of the template base dC at the n − 3 position (39%), or Asp540 (18%), which helps keep the position of the Lys592 side chain, and thus the DNA is fixed (Fig. 8A). Lys592 is equivalent to Lys706 of RB69 pol, which is similarly H-bonded with the n − 2 primer base and Asp621, but not with the n − 3 template base [9]. Lys706 and Asp621 of RB69 pol have been suggested to act as a sensor to detect wrongly incorporated nucleotides [9]. The extra H-bond between Lys592 and the n − 3 template base may provide additional stability and error sensitivity in Tgo pol.

3.7. The polymerase reaction and interactions with the incoming nucleotide

The incoming dTTP nucleotide triphosphate remains tightly bound to the catalytic Mg^{2+} ions in the polymerase active site. An additional, stable double H-bond is formed between the γ phosphate and Ser407 (Fig. 8A). Pi-stacking of the dTTP base with the primer 3′ terminal base is conserved throughout the simulation. However, base pairing between the dTTP base and its corresponding template base is frequently partially (70%) or completely (46%) broken. The dTTP phosphates make strong electrostatic interactions with helix P of the fingers. Asn491 is permanently H-bonded with the α phosphate, whereas Lys487 makes H-bonds with one or two of the three phosphates during the whole trajectory (Fig. 8). Lys487 is equivalent to Lys560 in RB69 pol, which is H-bonded with the dTTP triphosphate [9] and which has been identified as the general acid for protonation of the pyrophosphate leaving group during the second proton transfer of the polymerase reaction [26]. A possible alternative proton donor candidate is Arg460 in helix O of the fingers, which, although less strongly H-bonded with the β and/or γ phosphate (15%), is correlated with the opening-closing motion of the fingers domain.

Much less is known from literature about the proton acceptor in the first proton transfer, which is required to activate the O3′ atom of the primer 3′ terminus for nucleophilic attack on the dTTP Pα atom. The generally accepted catalytic role of Mg A is to lower the pKa of the primer 3′ hydroxyl to facilitate the initial proton transfer [27]. In the initial minimized ternary complex, the O3′ atom is at 0.20 nm distance from Mg A. However, during the simulation, O3′ only sporadically (0.8%) approaches Mg A below a 0.35 nm distance. Instead, the 3′ hydroxyl is a strong H-bond donor to the Asp540 carboxylate (56%) and a H-bond acceptor for the Thr541 hydroxyl (51%). In this doubly H-bonded state (41%), the average O3′–Mg A distance is 0.60 nm, yet the pi-stacking interaction between the primer 3′ base and dTTP remains intact (Fig. 8B). In conformations where a close interaction between O3′ and Mg A is present, the only candidate proton acceptor is the Thr541 hydroxyl, which itself is a H-bond donor to Asp540, which in turn forms a salt bridge with Lys592 (Fig. 8A). Thus, the MD data suggest a dual role for the Asp540–Thr541 duo. At close O3′–Mg A distance, a proton cascade starts from the primer 3′ hydroxyl to the Thr541 hydroxyl, which itself donates its proton to the Asp540 carboxylate. At about 0.6 nm distance, during the translocation step, strong H-bonds with Asp540 and Thr541 keep the primer 3′ hydroxyl in the vicinity of the catalytic center, while still allowing infrequent close O3′–Mg A encounters, which are necessary for the initial proton transfer. Thus, in addition to the role of Asp540 in the mismatch sensing mechanism [9], a leading role seems to be reserved for Asp540 and Thr541 as proton acceptors in the first proton transfer, and additionally in the translocation step by shifting the primer 3′ equilibrium position close to the priming site. The 0.3–0.4 nm relocation of the primer 3′ hydroxyl toward Mg A may be an alternative candidate for the rate-limiting conformational change in the

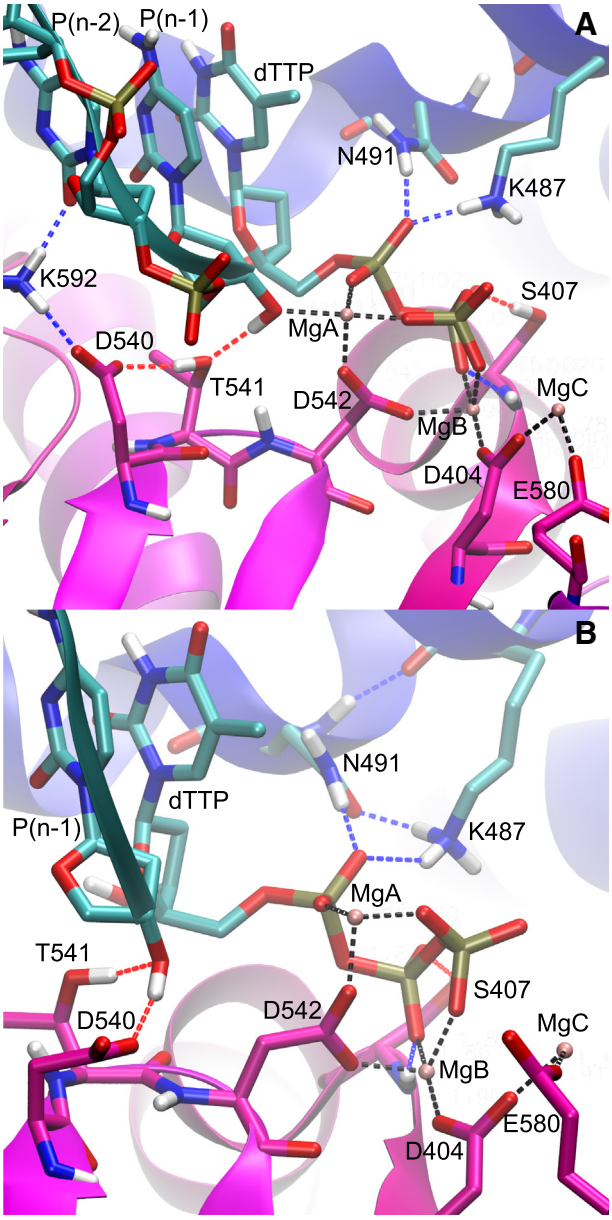

Fig. 8. Close-up view of the polymerase catalytic center. Two important conformational states are shown. (A) At a close primer O3′–Mg A distance, the system is ready for the first proton transfer reaction from the primer 3′ hydroxyl to the Thr541 side chain, which in turn donates a proton to Asp540. (B) When located at ~0.6 nm from Mg A, strong H-bonds with both Asp540 and Thr541 keep the primer O3′ in the vicinity of the reaction center. The blue and red dashed lines indicate H-bonds with the DNA and the incoming dTTP; the black dashed lines indicate electrostatic interactions with the Mg ions.

DNA polymerization reaction [25], given the sparsity of conformations with close O3′–Mg A distance.

4. Discussion

We have performed a benchmark REFT MD simulation of the ternary replicating complex comprising Tgo pol, primer–template DNA and incoming dTTP nucleotide. Starting from a closed apo conformation, PCA analysis of the protein and DNA dynamics shows a relaxation of the dsDNA from a twisted state to a partially untwisted state, which shows increased bending motion. This relaxation is assisted by the thumb domain moving toward the palm. Our results suggest that the sliding of the DNA occurs through correlated dsDNA-thumb motions, followed by repositioning of the thumb on the dsDNA chain to prepare for the next translocation step. While sliding across the polymerase active site, the dsDNA may locally switch back and forth between the stretched B-DNA conformation and the more compact AB-form or A-form. The increased bending and stretching flexibility of the dsDNA at the template 3′ end allows the formation and breaking of salt bridges with the cationic side chains to occur gradually, thus staying tightly bound to the enzyme.

The hypothesis that the thumb assists the sliding of the DNA is supported by the protein–DNA interactions; most cationic side chains that make important salt bridges with the dsDNA are located in the thumb domain. Experimental evidence for this mechanism is found in an engineered Tgo pol mutant capable of generating full-length 1′,5′-anhydrohexitol nucleic acid (HNA) from a DNA template strand [28]. All 14 mutations of this enzyme are located in the thumb, and several of the mutated residues make strong interactions with the primer strand, demonstrating the importance of the thumb domain for DNA replication.

The ability to adopt a B-DNA conformation at the n − 2 to n − 4 sites may be a strong requirement for continuous primer elongation. Evidence for this is found in the polymerization of synthetic DNA by wild-type DNA polymerases. HNA is a conformationally restricted RNA analog that adopts an A-form duplex [29]. The selective incorporation of HNA nucleotides into a DNA primer strand by the archaeal family B *Thermococcus litoralis* exo(-) pol stalls after the first two nucleotides [30]. This stalling effect is located right before the dinucleotide step with the highest preference for the B-form (Fig. 3). Locked nucleic acids (LNA) contain a ribose analog that is locked into a 3′-endo conformation, which induces A-like nucleic acid conformations [31]. Similar to HNA, after initial incorporation of this nucleotide analog by the archaeal family B *Pyrococcus furiosis*, further extension of the LNA polymer chain was stalled [32].

Protein-induced B-to-A conformational transition and attendant widening of the minor groove have been observed in many crystal structures of DNA-binding proteins [24]. In HIV-1 reverse transcriptase and most family A pols, A-like conformations are located immediately adjacent to the insertion site [24]. These conformational changes are thought to enable base pair mismatch detection through stiffening of the A-DNA backbone [33]. In family B (static) crystal structures, A-DNA conformations have not been observed. In the solvated complex however, conformational samples are distributed over the full A-B range, supporting the proposition of a dynamic role of the B-to-A transition.

Our PCA analysis suggests that dsDNA bending may be induced by partial untwisting. Experimentally, bending is indeed correlated with untwisting in many complexes with DNA-bending proteins [34]. Additional support for untwisting-induced bending was given by MD simulations on several dsDNA sequences in aqueous solvent [35]. By applying restraints at different values the twist angle, it was shown that the average bend angle increased with decreasing twist angle.

Comparison with the PCA of reported archaea polymerase crystal structures suggests that the enzyme can be in three overall conformational states, which represent their functional state: an open state in the apo enzyme; a closed state in the replicating complex; and an extremely closed donut-like state in the editing complex. Interconversion between these states requires collective motions involving rotation of the fingers and thumb toward the palm. While in the mesophilic RB69 pol analog, the fingers motion is independent from the rest of the protein, the motion of the fingers occurs in concert with the exo and N-term domains.

According to the MD data, the conserved Asp540 and Thr541 side chains play a dual catalytic role in the DNA polymerization. In the chemical step, they act as proton acceptors in the initial proton transfer cascade. In the DNA translocation step, they form strong H-bonds with the primer 3′ hydroxyl, which shifts the equilibrium position of the primer 3′ terminus close to the priming site. Asp540 and Thr541 are part of the conserved motif C (YADTDG) [36], and are strictly conserved among family B DNA polymerases [8]. Site-directed mutagenesis experiments have shown that the equivalent amino acids in phi29 pol and human pol α are essential for polymerase activity [37–39].

While the Watson–Crick base pairing of the primer–template dsDNA remains intact, the fraction of conformations with Watson–Crick H-bonding of the nascent base pair is relatively low. This finding is consistent with the work of Morales and Kool [40], who replaced natural bases with nonpolar isosteric analogs lacking Watson–Crick H-bonding ability. Several pols, including the family B pol α, were able to incorporate the nonnatural base pairs with high efficiency, demonstrating that H-bonding between the base pairs is not strictly necessary at the insertion site, on the condition that the geometry of the base pair and specific minor groove interactions with the protein are conserved. Base pairing is necessary, however, at the n − 2 and n − 3 sites to form a strong H-bonded network with Lys592 and Asp540, which cooperatively act as a DNA mismatch sensor and locally restrain the DNA to the B-DNA conformation. Indeed, primer extension by the exo(-) variant of the closely related Vent pol from *T. litoralis* at an abasic site has been shown to yield largely one-base extension products, thus stalling at site n − 1 [41].

5. Conclusion

We have shown that the REFT method enables exploration of the native state conformational space of a large-sized (750-residue) protein, a Tgo pol–DNA replication complex, and the investigation of its cooperative dynamics. We have found strong correlation between DNA flexibility and the thumb motion, which directly determines the processivity. The protein–DNA interaction strongly influences the shape of the DNA: increased preference for the B-DNA conformation is seen at the n − 2 to n − 4 steps, while the tendency to adopt more A-like conformations is greater at larger distances from the insertion site. These findings have important implications for the design of polymerases capable of synthesizing polymers from artificial nucleic acids.

Acknowledgement

This research was conducted utilizing high-performance computational resources provided by the University of Leuven (http://ludit.kuleuven.be/hpc). This work was funded by the KU Leuven IDO project 3E100304.

Appendix A. Supplementary data

Supplementary data to this article can be found online at http://dx.doi.org/10.1016/j.bbapap.2013.09.003.

References

[1] J. Cline, J.C. Braman, H.H. Hogrefe, Pcr fidelity of pfu dna polymerase and other thermostable dna polymerases, Nucleic Acids Res. 24 (1996) 3546–3551.
[2] D. Loakes, P. Holliger, Polymerase engineering: towards the encoded synthesis of unnatural biopolymers, Chem. Commun. (2009) 4619–4631.

[3] S. Yang, P. Herdewijn, Polymerase-dependent dna synthesis from phosphoramidate-activated nucleotides, Nucleosides Nucleotides Nucleic Acids 30 (2011) 597–608.
[4] N. Ramsay, A. Jemth, A. Brown, N. Crampton, P. Dear, P. Holliger, cyDNA: synthesis and replication of highly cy-dye substituted DNA by an evolved polymerase, J. Am. Chem. Soc. 132 (2010) 5096–5104.
[5] R. Radhakrishnan, T. Schlick, Orchestration of cooperative events in DNA synthesis and repair mechanism unraveled by transition path sampling of DNA polymerase beta's closing, Proc. Natl. Acad. Sci. U. S. A. 101 (2004) 5970–5975.
[6] A.A. Golosov, J.J. Warren, L.S. Beese, M. Karplus, The mechanism of the translocation step in DNA replication by DNA polymerase I: a computer simulation analysis, Structure 18 (2010) 83–93.
[7] L. Da, D. Wang, X. Huang, Dynamics of pyrophosphate ion release and its coupled trigger loop motion from closed to open state in RNA polymerase II, J. Am. Chem. Soc. 134 (2011) 2399–2406.
[8] K.P. Hopfner, A. Eichinger, R.A. Engh, F. Laue, W. Ankenbauer, R. Huber, B. Angerer, Crystal structure of a thermostable type b DNA polymerase from *Thermococcus gorgonarius*, Proc. Natl. Acad. Sci. U. S. A. 96 (1999) 3600–3605.
[9] M.C. Franklin, J. Wang, T.A. Steitz, Structure of the replicating complex of a pol alpha family DNA polymerase, Cell 105 (2001) 657–667.
[10] S.J. Firbank, J. Wardle, P. Heslop, R.J. Lewis, B.A. Connolly, Uracil recognition in archaeal DNA polymerases captured by x-ray crystallography, J. Mol. Biol. 381 (2008) 529–539.
[11] B. Hess, C. Kutzner, D. van der Spoel, E. Lindahl, Gromacs 4: algorithms for highly efficient, load-balanced, and scalable molecular simulation, J. Chem. Theory Comput. 4 (2008) 435–447.
[12] K. Lindorff-Larsen, S. Piana, K. Palmo, P. Maragakis, J.L. Klepeis, R.O. Dror, D.E. Shaw, Improved side-chain torsion potentials for the amber ff99sb protein force field, Proteins 78 (2010) 1950–1958.
[13] A. Perez, I. Marchan, D. Svozil, J. Sponer, T.E. Cheatham, C.A. Laughton, M. Orozco, Refinement of the amber force field for nucleic acids: improving the description of alpha/gamma conformers, Biophys. J. 92 (2007) 3817–3829.
[14] K.L. Meagher, L.T. Redman, H.A. Carlson, Development of polyphosphate parameters for use with the amber force field, J. Comput. Chem. 24 (2003) 1016–1025.
[15] S.L.C. Moors, S. Michielssens, A. Ceulemans, Improved replica exchange method for native-state protein sampling, J. Chem. Theory Comput. 7 (2011) 231–237.
[16] P. Liu, B. Kim, R.A. Friesner, B.J. Berne, Replica exchange with solute tempering: a method for sampling biological systems in explicit water, Proc. Natl. Acad. Sci. U. S. A. 102 (2005) 13749–13754.
[17] X. Huang, M. Hagen, B. Kim, R.A. Friesner, R. Zhou, B.J. Berne, Replica exchange with solute tempering: efficiency in large scale systems, J. Phys. Chem. B 111 (2007) 5404–5410.
[18] D.J. Jacobs, A.J. Rader, L.A. Kuhn, M.F. Thorpe, Protein flexibility predictions using graph theory, Proteins 44 (2001) 150–165.
[19] D. Petrey, Z. Xiang, C.L. Tang, L. Xie, M. Gimpelev, T. Mitros, C.S. Soto, S. Goldsmith-Fischman, A. Kernytsky, A. Schlessinger, I.Y.Y. Koh, E. Alexov, B. Honig, Using multiple structure alignments, fast model building, and energetic analysis in fold recognition and homology modeling, Proteins 53 (Suppl. 6) (2003) 430–435.
[20] R. Lavery, M. Moakher, J.H. Maddocks, D. Petkeviciute, K. Zakrzewska, Conformational analysis of nucleic acids revisited: curves+, Nucleic Acids Res. 37 (2009) 5917–5929.
[21] X. Lu, W.K. Olson, 3dna: a versatile, integrated software system for the analysis, rebuilding and visualization of three-dimensional nucleic-acid structures, Nat. Protoc. 3 (2008) 1213–1227.
[22] S. Hayward, R.A. Lee, Improvements in the analysis of domain motions in proteins from conformational change: DynDom version 1.50, J. Mol. Graph. Model. 21 (2002) 181–183.
[23] T. Killelea, S. Ghosh, S.S. Tan, P. Heslop, S.J. Firbank, E.T. Kool, B.A. Connolly, Probing the interaction of archaeal DNA polymerases with deaminated bases using X-ray crystallography and non-hydrogen bonding isosteric base analogues, Biochemistry 49 (2010) 5772–5781.
[24] X.J. Lu, Z. Shakked, W.K. Olson, A-form conformational motifs in ligand-bound DNA structures, J. Mol. Biol. 300 (2000) 819–840.
[25] J.A. Brown, Z. Suo, Elucidating the kinetic mechanism of DNA polymerization catalyzed by *Sulfolobus solfataricus* p2 DNA polymerase b1, Biochemistry 48 (2009) 7502–7511.
[26] C. Castro, E.D. Smidansky, J.J. Arnold, K.R. Maksimchuk, I. Moustafa, A. Uchida, M. Gotte, W. Konigsberg, C.E. Cameron, Nucleic acid polymerases use a general acid for nucleotidyl transfer, Nat. Struct. Mol. Biol. 16 (2009) 212–218.
[27] M. Fothergill, M.F. Goodman, J. Petruska, A. Warshel, Structure-energy analysis of the role of metal ions in phosphodiester bond hydrolysis by DNA polymerase I, J. Am. Chem. Soc. 117 (1995) 11619–11627.
[28] V.B. Pinheiro, A.I. Taylor, C. Cozens, M. Abramov, M. Renders, S. Zhang, J.C. Chaput, J. Wengel, S. Peak-Chew, S.H. McLaughlin, P. Herdewijn, P. Holliger, Synthetic genetic polymers capable of heredity and evolution, Science 336 (2012) 341–344.
[29] R. Declercq, A.V. Aerschot, R.J. Read, P. Herdewijn, L.V. Meervelt, Crystal structure of double helical hexitol nucleic acids, J. Am. Chem. Soc. 124 (2002) 928–933.
[30] K. Vastmans, S. Pochet, A. Peys, L. Kerremans, A. Van Aerschot, C. Hendrix, P. Marliere, P. Herdewijn, Enzymatic incorporation in DNA of 1,5-anhydrohexitol nucleotides, Biochemistry 39 (2000) 12757–12765.
[31] K. Bondensgaard, M. Petersen, S.K. Singh, V.K. Rajwanshi, R. Kumar, J. Wengel, J.P. Jacobsen, Structural studies of LNA:RNA duplexes by NMR: conformations and implications for RNase h activity, Chemistry 6 (2000) 2687–2695.
[32] R.N. Veedu, B. Vester, J. Wengel, In vitro incorporation of LNA nucleotides, Nucleosides Nucleotides Nucleic Acids 26 (2007) 1207–1210.
[33] Y. Timsit, DNA structure and polymerase fidelity, J. Mol. Biol. 293 (1999) 835–853.
[34] S. Jones, R. van Heyningen, H. Berman, J. Thornton, Protein–DNA interactions: a structural analysis, J. Mol. Biol. 287 (1999) 877–896.
[35] S. Kannan, K. Kohlhoff, M. Zacharias, B-DNA under stress: over- and untwisting of DNA during molecular dynamics simulations, Biophys. J. 91 (2006) 2956–2965.
[36] M. Delarue, O. Poch, N. Tordo, D. Moras, P. Argos, An attempt to unify the structure of polymerases, Protein Eng. 3 (1990) 461–467.
[37] A. Bernad, L. Blanco, M. Salas, Site-directed mutagenesis of the ycdtds amino acid motif of the phi 29 dna polymerase, Gene 94 (1990) 45–51.
[38] M.A. Blasco, A. Bernad, L. Blanco, M. Salas, Characterization and mapping of the pyrophosphorolytic activity of the phage phi 29 DNA polymerase. involvement of amino acid motifs highly conserved in alpha-like DNA polymerases, J. Biol. Chem. 266 (1991) 7904–7909.
[39] W.C. Copeland, T.S. Wang, Mutational analysis of the human DNA polymerase alpha. The most conserved region in alpha-like DNA polymerases is involved in metal-specific catalysis, J. Biol. Chem. 268 (1993) 11028–11040.
[40] J.C. Morales, E.T. Kool, Varied molecular interactions at the active sites of several DNA polymerases: nonpolar nucleoside isosteres as probes, J. Am. Chem. Soc. 122 (2000) 1001–1007.
[41] S. Lim, I. Song, F.P. Guengerich, J. Choi, Effects of n(2)-alkylguanine, o(6)-alkylguanine, and abasic lesions on DNA binding and bypass synthesis by the euryarchaeal b-family DNA polymerase vent (exo(-)), Chem. Res. Toxicol. 25 (2012) 1699–1707.